RSC Advances

PAPER

View Article Online
View Journal | View Issue

Cite this: *RSC Adv.*, 2017, **7**, 35757

The peak shift and evolution of upconversion luminescence from $CsPbBr_3$ nanocrystals under femtosecond laser excitation

Qiuju Han, [ab] Wenzhi Wu, [c] Weilong Liu [a] and Yanqiang Yang *[a]

The luminescent characteristics of $CsPbBr_3$ nanocrystals in *n*-hexane are investigated by the use of steady-state/time-resolved photoluminescence and transient absorption spectroscopy. Compared with normal luminescence, a redshift of the upconversion luminescence (UCL) spectrum under 800 nm femtosecond laser excitation is observed. Time-resolved PL and TA spectroscopy under near-infrared femtosecond laser excitation demonstrate that the full width at half maximum and peak position are changed at various delay times, suggesting the existence of more than a single excited state. It is found that UCL is composed of a photoinduced surface-trapping and a band-edge excitonic state, causing the observed biexponential dynamics. We conclude that the redshift of the emission peak is caused by the relative change in luminescent intensity between excitonic and trapping states.

Received 3rd June 2017
Accepted 23rd June 2017

DOI: 10.1039/c7ra06211g

rsc.li/rsc-advances

1. Introduction

Halide perovskite nanocrystals (NCs) have attracted intensive attention due to their strikingly high light-harvesting efficiency in solar energy applications and their function as light-absorbing direct-bandgap semiconductor materials in the last several years.[1–3] Furthermore, these new NCs are also found to be excellent light-emitting materials, manifesting unique performance in electrically driven light-emitting diodes (LEDs), optically pumped lasers and quantum dot displays.[4–7] Halide perovskite semiconductor NCs have recently been synthesized to further promote their optoelectronic performance with the aid of the quantum confinement effect, which ensures superior photoluminescence quantum yield (PLQY) stabilized by ligands.[8] Stable excitons or hole–electron pairs are created in cesium-based perovskite NCs at room temperature even under low-intensity light excitation, and they present high PLQY of up to 90% without any further surface treatments.[6] Upconversion luminescence (UCL) is a well-known phenomenon that refers to nonlinear optical processes based on the sequential absorption of two or more photons through virtual or real intermediate energy states, leading to emission of higher energy photons than the excitation photons. This is in contrast to normal photoluminescence (PL), where the emission wavelength has lower energy than the excitation wavelength.[9] The peak shift of PL spectra between normal luminescence and UCL is observed in most of II–VI NCs[10] and is explained by a two-state intensity-dependent model.[11] The UCL of NCs is mostly attributed to sub-band gap surface, metastable, or intermediate states;[12] furthermore, in order to achieve high PLQY, the concentration of the trap/defect states should be low to minimize nonradiative recombination. Two-photon excitation technique, a promising optical method, can be used to investigate the luminescent property of halide perovskite NCs, which are responsible for UCL under strong laser excitation. Amplified spontaneous emission from cesium-based perovskite NC films on substrate is observed under two-photon laser excitation.[3,5,13] Due to the highly ionic nature and good stoichiometry of halide perovskite NCs, point defects are not likely to reside within the volume of perovskite NCs.[14] However, the capping agent (*e.g.* octadecylamine, ODA) is likely to replace the organic or inorganic cation in the perovskite NCs, causing lattice disorder and surface-related trapping states at the surface region.[15,16] In the electronic structure calculation of cesium lead halide perovskite NCs, shallow surface trapping state would arise from a lead-rich surface.[17,18] Compared with normal luminescence, a redshift of UCL peak position in $CsPbBr_3$ NC solution or film can be easily observed.[5,13,19] There are scarce reports on the origin of emission peak shift between normal luminescence and UCL of $CsPbBr_3$ NCs. The nature of the trapping state needs to be systematically explored and further understood.

In this study, UCL of $CsPbBr_3$ NCs in *n*-hexane is investigated comparatively by the use of steady-state/time-resolved PL and transient absorption (TA) spectroscopy under femtosecond laser excitation. The change in spectra and lifetimes of transition components are observed and discussed. Time- and spectral-resolved data can give more information to illuminate

[a]*Department of Physics, Harbin Institute of Technology, Harbin, Heilongjiang, 150001, China. E-mail: yqyang@hit.edu.cn*

[b]*School of Science, Northeast Agricultural University, Harbin, Heilongjiang, 150030, China*

[c]*School of Electronic Engineering, Heilongjiang University, Harbin, Heilongjiang, 150080, China*

the mechanism of peak shift between normal luminescence and UCL in $CsPbBr_3$ NCs. Based on these experimental results, we intend to use an intensity-dependent energy level model to interpret the shift of the UCL emission peak in $CsPbBr_3$ NCs.

2. Experimental

2.1. Synthesis and preparation

$CsPbBr_3$ NCs are synthesized with a hot-injection approach. Oleylamine and oleic acid are injected at 120 °C under N_2 condition. $PbBr_2$ and octadecene are loaded into a 50 mL 3-necked flask and degassed at 120 °C for 30 min. After complete solubilisation of $PbBr_2$ salt, the temperature is raised to 160 °C. Cs-oleate solution is obtained by dissolving $CsCO_3$ in octadecene and oleic acid at 150 °C, which is then quickly injected into the mixture. After 5 seconds, the reaction mixture is cooled using an ice-water bath, and $CsPbBr_3$ NCs in *n*-hexane are readily obtained. The PLQY of the $CsPbBr_3$ NCs is higher than 80%. High-resolution transmission electron microscope (TEM) measurement is performed on a Tecnai G220 S-Twin microscope operating at a high voltage of 200 kV. We collected the ground-state absorption spectrum of $CsPbBr_3$ NCs on a Persee TU-190 vis/NIR spectrometer.

2.2. Experimental sections

A femtosecond Ti: sapphire regenerative amplifier (Coherent, Legend) produces ~120 fs pulses at 1.55 eV (800 nm) and 1 kHz. A second harmonic β-barium borate (BBO) crystal is used to double the photon energy of the laser pulse to 3.10 eV (400 nm), after which a band-pass filter is used to block the residual laser beam at 1.55 eV.

2.2.1. Steady-state PL spectrum. The emission and scattered light of the sample in the vertical direction of the laser is collected by a spectrometer (iHR550, Horiba) and detected by a charge-coupled device (CCD). Power variations are adjusted using an energy attenuator and measured with a power meter. Laser pulses are focused on the sample to a spot size of 3.02 mm, which is measured by the scanning knife-edge technique. The intensity of the 400 nm pump pulse energy is varied from 7.14×10^{-3} to 4.29×10^{-1} mJ cm^{-2}. Temperature-dependent steady-state PL measurements are performed *via* a vacuum liquid-nitrogen cryostat (Orient, KOJI) with a temperature controller (TC202, East Changing).

2.2.2. Nanosecond time-resolved PL spectroscopy. Time-resolved luminescence spectra are measured on a spectrometer (PI instruments, SP-2500) with an intensified CCD detector (PI instruments). Instrument response time is 2.0 ns when scattering light pulses are measured. Due to the average PL lifetime (~10 ns) of $CsPbBr_3$ NCs and the limitation of instrument response time for ICCD, time-correlated single-photon counting (TCSPC, Boston Electronics) can also provide detailed information about the dynamics with the time resolution of 60 ps scale in real time. The system consists of a monochromator (SSM101, Zolix) equipped with a detector (id100-50, ID Quantique) and a single-photon counting electronics module (SPC-130, Becker & Hickl GmbH) accounting for data acquisition. A supercontinuum picosecond laser (Surperk Extreme EXB-4, NKT Photonics) is employed as the excitation source; the optical wavelengths of 400 nm or 800 nm are used to excite the samples, respectively.

2.2.3. TA spectroscopy. A pump beam at 400 nm or 800 nm was used in all the TA measurements in this study. Laser pulses at 800 nm are focused onto a sapphire window with a thickness of 2 mm to produce white continuum light (WCL) extending from 380 to 800 nm, which is divided into the probe beam and the reference beam. The intensity of 800 nm laser pulse is adjusted by an iris and a neutral density filter to obtain a stable WLC probe beam. The probe beam is focused onto the quartz cuvette (optical path of 1 mm) containing $CsPbBr_3$ NC solution with a spot size of 1 mm, and the pump beam spot is ~2 mm in diameter. Pump and probe beams are overlapped spatially at the sample position. Detection of the probe pulses was done with and without pump using a 500 Hz mechanical chopper. Two highly sensitive spectrometers (Avantes-950F) are used to collect the probe and reference beams for recording and calculating the TA dynamic traces. The relative delay between the pump and probe pulse is controlled with the help of a stepper motor-driven optical delay line (Zolix, TSA-200). A series of experiments have been performed with the pump fluence changed using an energy attenuator. The sample is placed in a quartz cuvette (1 mm) in order to reduce ground-state absorption processes.

3. Results and discussion

3.1. Optical and structural characterization

The $CsPbBr_3$ NCs in *n*-hexane have their first absorption peaks at 506 nm, which corresponds to the band-edge excitonic absorption, as shown in Fig. 1(a). The peaks are blue shifted from the energy gap of bulk $CsPbBr_3$ material at 551 nm.[20] Electronic transitions in the centers of $CsPbBr_3$ NCs couple to vibrations, which result in a broadening of absorption and emission bands as well as a Stokes shift (15 nm).[21] A bathochromic effect is shown in the luminescence spectra. The redshift of the emission peaks is about 13 meV (3 nm) between the 800 nm and 400 nm femtosecond laser excitation. The location of the emission peak does not change with various laser intensities, but a redshift is observed at various excitation wavelengths for $CsPbBr_3$ NCs in close-packed films[5] and toluene.[19] A shift of the emission peak is observed. Some researchers think the slight redshift of two-photon excitation can be ascribed to the reabsorption effect and the size distribution for traditional II–VI NCs[22] and carbon quantum dots. The following mechanism of reabsorption is demonstrated: an incoming photon with energy of $h\nu_0$ is absorbed by a smaller NC in the solution, and after a delay, this excited NC emits a second photon with a smaller energy of $h\nu_1$ due to the Stokes shift. This photon is then absorbed by a larger NC in the solution; after a similar delay, this NC emits a third photon with an even smaller energy of $h\nu_2$, and this photon will escape from the solution and contribute to the measured PL. The frequent occurrence of photon reabsorption results in a decrease in the emission of the smaller NCs and an increase in the emission of

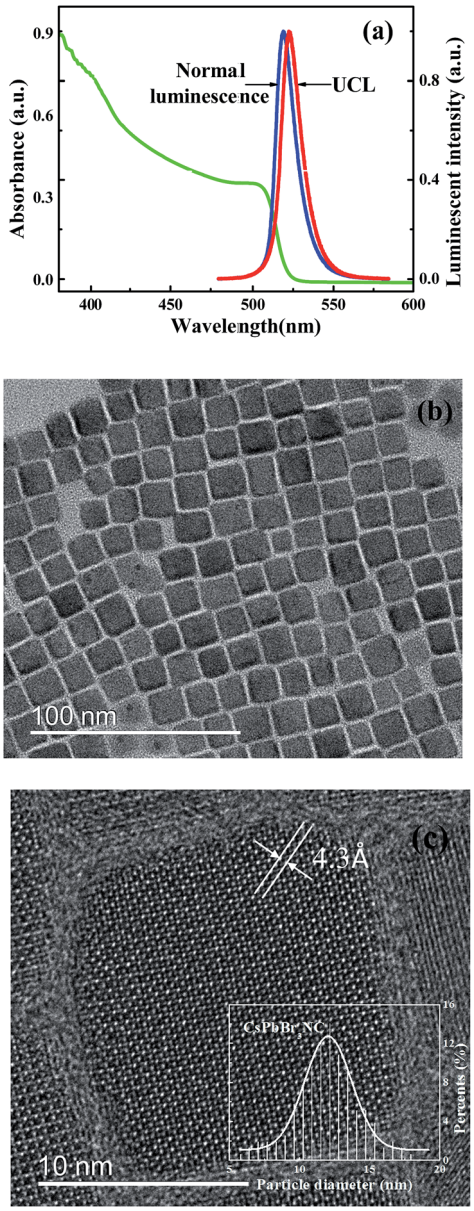

Fig. 1 (a) Absorption and PL spectra of $CsPbBr_3$ NCs in *n*-hexane. (b) Typical TEM images of perovskite $CsPbBr_3$ NCs. (c) High-resolution TEM photograph of the individual particle, inset is the size distribution of perovskite $CsPbBr_3$ NCs.

the larger ones.[23] In other words, the emission peak wavelength in time-resolved PL spectroscopy should have a redshift with a longer delay time. Transmission electronic microscopy (TEM) images of the perovskite QDs are presented in Fig. 1(b). Fig. 1(c) shows the TEM image of an individual perovskite $CsPbBr_3$ NC with the lattice fringe of 4.3 Å. Because of their deviation from cubic shape, the sizes of $CsPbBr_3$ NCs measured along their edges are 12.0 nm, which is consistent with the curve calculated using effective mass approximation.[6] The band gap of the sample is 2.45 eV at room temperature. Meanwhile, full widths at half maximum (FWHMs) of the PL spectra are ~20 nm.[24,25]

The variation in the UCL spectra of $CsPbBr_3$ NC films is examined the under excitation wavelength of 800 nm at various

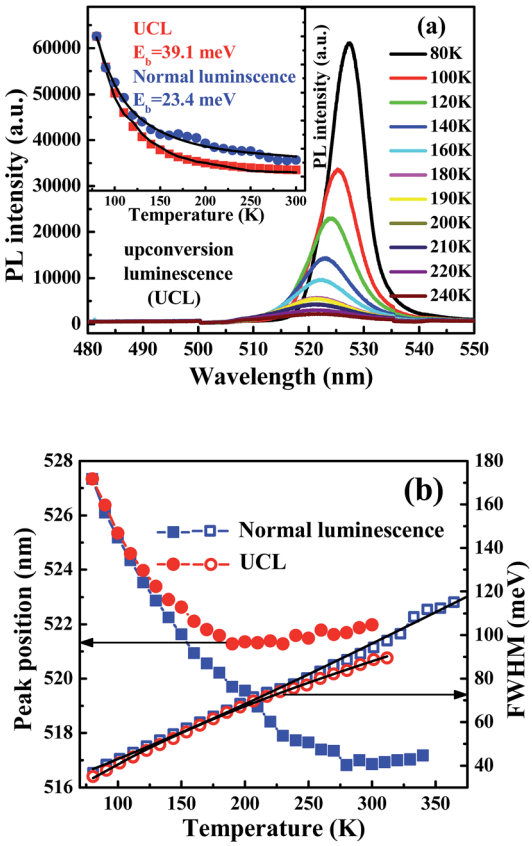

Fig. 2 (a) Temperature-dependent UCL spectra of $CsPbBr_3$ NC films at 80–240 K. Inset is the PL intensity of $CsPbBr_3$ NC films as a function of temperature. (b) Peak position and linewidths of $CsPbBr_3$ NC films as a function of temperature.

temperatures in the range 80–240 K, as shown in Fig. 2(a). The NC films exhibit a decrease in the PL intensity with increasing temperature. Besides, the peak energies of these NC films shift to the higher energy side, and the PL emission linewidths significantly increase with increasing temperature. The UCL intensity gradually decreases with increasing the temperature to 300 K, indicating thermal quenching of UCL emission. The intensities of UCL and normal luminescence as a function of temperature are fitted as shown in Fig. 2(b) by using the Arrhenius equation,[26,27] $I(T) = I_0/(1 + A\exp(E_b/k_BT))$, in which I_0 is the intensity at 80 K, A is a constant related to the ratio between the radiative and nonradiative lifetimes, E_b is the thermal quenching energy, and k_B is the Boltzmann constant. The obtained thermal quenching energy of UCL is 39.1 meV, which is bigger than that of normal luminescence at 23.4 meV. The thermal quenching energy can be considered to be the exciton binding energy if no other nonradiative decay channel is in the exciton recombination process in the all-inorganic perovskite NCs.[28] The temperature-dependent PL linewidth is fitted using the independent Boson model as[29]

$$\Gamma(T) = \Gamma_0 + \Gamma_{op}/(e^{\hbar\omega_{op}/k_BT} - 1) \quad (1)$$

where Γ_0 is the inhomogeneous broadening contribution, Γ_{op} is the exciton-optical phonon contribution to the linewidth broadening, and $\hbar\omega_{op}$ is the longitudinal optical-phonon energy. The first term dominates in eqn (1) at relatively low temperature, and a nearly constant broadening is expected. $\hbar\omega_{op}$ is determined to be 40.6 and 44.1 meV for 400 and 800 nm femtosecond laser excitation, respectively. The UCL and normal luminescence peak, as well as the FWHM of $CsPbBr_3$ NC films at various temperatures, are shown in Fig. 2(b). With further increase of the temperature above 230 K, the FWHM of UCL becomes smaller than that of normal luminescence. Moreover, the wavelengths of the emission peak between normal luminescence and UCL become different with the temperature increase. These changes may be related to the trapping states appearing at higher temperatures, which may indicate that there are two decay channels (excitons and trapping carriers) at high temperature.[30] More recently, the photoactivation of $CsPbBr_3$ NCs and blinking of single dots have revealed the existence of defects or trapping states in the NCs.[31]

3.2. Power dependence of steady-state PL under femtosecond laser excitation

Strong UCL of $CsPbBr_3$ NCs in *n*-hexane is observed when 800 nm femtosecond laser pulses pass through the NC solution, as shown in the inset of Fig. 3. At the same experimental conditions, we can see strong absorption and scattering luminescence under 400 nm femtosecond laser excitation. The UCL intensity has a slope of 1.80 at 800 nm excitation, while the normal luminescence intensity has a slope of 0.89, as shown in Fig. 3. The results indicate that normal luminescence intensity is linearly dependent on excitation power, whereas UCL intensity varies quadratically with pump power. It is therefore concluded that UCL is attributed to two-photon excitation.

3.3. Nanosecond luminescence dynamics

Time-resolved nanosecond luminescence dynamics has been widely applied to the investigation of the nanocrystalline structure and excited-state photophysics. In order to study the luminescent mechanism of $CsPbBr_3$ NCs and determine the cause for the peak of PL spectra, we examined the luminescence dynamics of $CsPbBr_3$ NCs in solution under 400 nm and 800 nm laser excitation. The luminescence dynamics was measured using TCSPC at the wavelength of 520 nm with a band-pass filter. The average lifetimes of normal luminescence and UCL are 9.3 and 12.7 ns, respectively. Decay data show that the dynamic process consists of a fast component and a slow component attributed to the excitonic state and the charge trapping state, respectively.[32,33] The fast component, with lifetimes much shorter than those of conventional $CH_3NH_3PbBr_3$ NCs, indicates that there is one band-edge exciton recombination process.[10] The slow component can be attributed to the intrinsic trap-free charge recombination, which is sensitive to temperature and detection wavelength. Time-resolved UCL decays of the $CsPbBr_3$ NCs show longer average lifetime of 12.7 ns than that of normal PL, which was measured at 9.3 ns. Two different timescales are assigned to the excitonic state emission together with trapping state emission, fitted with a fast lifetime of 3.6 ns at ratio of 39% and a slow lifetime of 18.4 ns at the ratio of 61%. It is interesting to note that the trapping components of UCL have a bit longer lifetimes than those of normal luminescence, as shown in Fig. 4(a). Time-resolved normal luminescence and UCL spectra are also measured with ICCD under 400 nm and 800 nm laser excitation, respectively. If the redshift of emission spectra from normal luminescence to UCL is dominated by reabsorption, the emission peak wavelength of time-resolved PL spectroscopy should have a redshift with the longer delay time. However, an opposite tendency on spectral shift exists for $CsPbBr_3$ NCs. A peak shift of ~2 nm between 0 and 6.5 ns can be observed for normal luminescence, as shown in Fig. 4(b); time-resolved UCL spectra indicate that the obvious blue shift of emission peaks of about 3 nm is observed at 0 and 6.5 ns, as shown in Fig. 4(b). With delay time increasing, FHWMs of UCL spectra are changed from 19.5 to 18.5 nm; however, FWHMs of normal luminescence are changed from 16.5 to 15.5 nm, as shown in Fig. 4(c). The change in peak positions at various delay times indicates the involvement of more than a single excited state. The peak shifts are attributed to the changes in emission intensity ratio of the surface trapping and excitonic state on the conduction band edge at various temporal evolutions. Furthermore, the trapping and excitonic emission peaks are close to each other, so we cannot distinguish one from the other by their profiles and line shapes.[11,34] The faster component is easily observed, even though much lower laser fluence (0.06 μJ cm^{-2}) was used. This confirms our assignment of this component as arising from excitonic emission rather than through an Auger-assisted recombination process.[34]

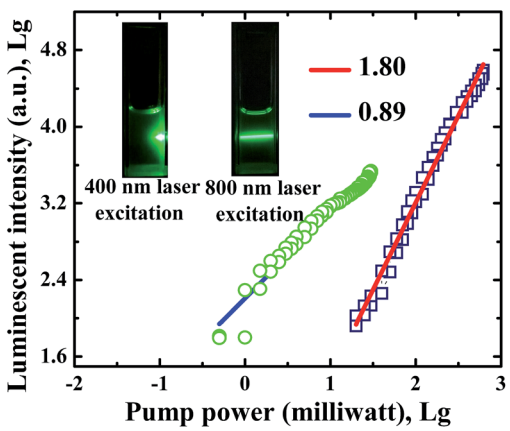

Fig. 3 Dependence of the luminescent intensity in $CsPbBr_3$ NCs on the pump power. The inset shows the photographs of $CsPbBr_3$ NCs in *n*-hexane under 400 and 800 nm femtosecond laser excitation.

The percentage of trapping luminescence changes when the wavelength of laser excitation is changed from 400 to 800 nm. According to our assumption, the redshift of UCL is produced by the change in the relative intensity of excitonic and trapping states at one- or two-photon excitation. We describe this behaviour with the aid of the schematics in Scheme 1. There, the thickness of the solid lines represents the luminescence

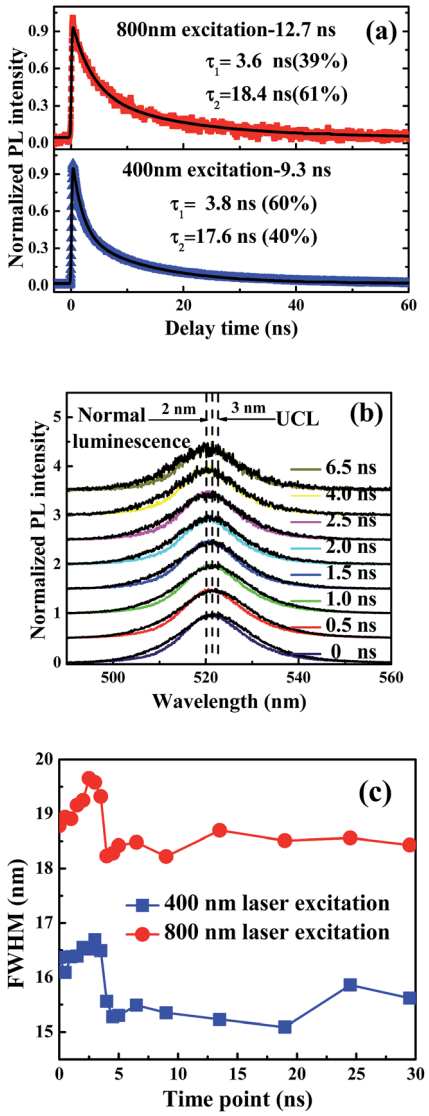

Fig. 4 (a) Time-resolved PL curves of $CsPbBr_3$ in *n*-hexane with laser excitation at 400 and 800 nm, respectively. (b) Nanosecond time-resolved normal luminescence (color lines) and UCL (black solid lines) spectra from bottom to top, for $t = 0$, 0.5, 1.0, 1.5, 2.0, 2.5, 4.0 and 6.5 ns. There is a 2 and 3 nm shift (vertical lines) to higher energy over time for the 400 and 800 nm laser excitation, respectively. (c) FWHMs of PL spectra are calculated at various time points.

intensity. When the sample is photoexcited with the photon energy of $h\nu$, two recombination pathways emerge for photo-induced electrons due to the existence of trapping and excitonic states. The two excited states have various dependences on the wavelength of laser excitation, so the change in the relative intensity can cause a redshift of the emission peak of UCL.

3.4. Carrier dynamics by TA

TA and optical Kerr shutter measurement can provide further information on excitation dynamics at the subpicosecond timescale.[35] In order to understand trapping states and the UCL mechanism of $CsPbBr_3$ NCs, TA measurement in $CsPbBr_3$ NCs is performed under 400 nm and 800 nm femtosecond laser

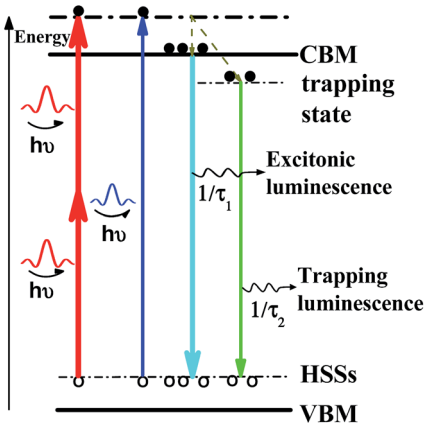

Scheme 1 Schematic energy level diagram to illustrate the luminescent mechanism of $CsPbBr_3$ NCs with trapping and excitonic states originated in quantum confinement. CBM: conduction band minimum; ESSs: electron surface states; HSSs: hole surface states; VBM: valance band maximum.

excitation, respectively. Qualitatively different TA dynamics can be found when the excitation density is much more than one exciton per NC, which is calculated in terms of absorption cross section and Poisson distribution.[36] Pump photon fluxes are controlled to generate the same number of excitons per particle at a low excitation level, which corresponds to mean excitation numbers per NCs $\langle N \rangle$, as estimated based on the absorption cross-section (σ) recorded at special wavelength and pulse fluence (j, photons per cm^2): $\langle N \rangle = \sigma j$. Here, the excitation energy of the laser pulse is adjusted to ensure the mean excitation numbers per NC solution $\langle N \rangle$ remains from 0.2 to 3.0, which is comparable with the excitation laser power for time-resolved PL measurement. An approximately symmetric spectral shape of UCL can be obtained under 800 nm femtosecond laser excitation. Here, pump power under 800 nm laser excitation is ten times that of 400 nm laser excitation to get the same luminescent intensity, which is used in time-resolved PL measurement. However, the spatial evolution of TA for $CsPbBr_3$ NCs is asymmetrical and complicated. Fig. 5(a) and (b) show time-resolved $\Delta A/A$ spectra of $CsPbBr_3$ NCs under 400 nm and 800 nm laser excitation, respectively.[37] The delay time ranges from −3.0 ps to 602.0 ps, and the arrows indicate the evolution of the delay time. We can see that the spectral response of $CsPbBr_3$ NCs shows three components with various time scales, including a long photoinduced transient bleach at ~510 nm, a quick excited state absorption (EAS) in the range of 470–490 nm and an additional TA signal at ~525 nm. The negative transient bleach signal at ~510 nm is assigned to ground-state depopulation, as its peak matches with the first excitonic absorption peak, which is due to the filling of band-edge states. Photoinduced luminescence, which is difficult to completely rule out, has a weak influence on this negative bleach signal.[38] The positive TA signal at 470–490 nm and 520 nm is assigned to photoinduced absorption of excited states, which show a similar monotonic decay behaviour and relaxation time.[39] Consistent with the proposed theory, the charge carrier

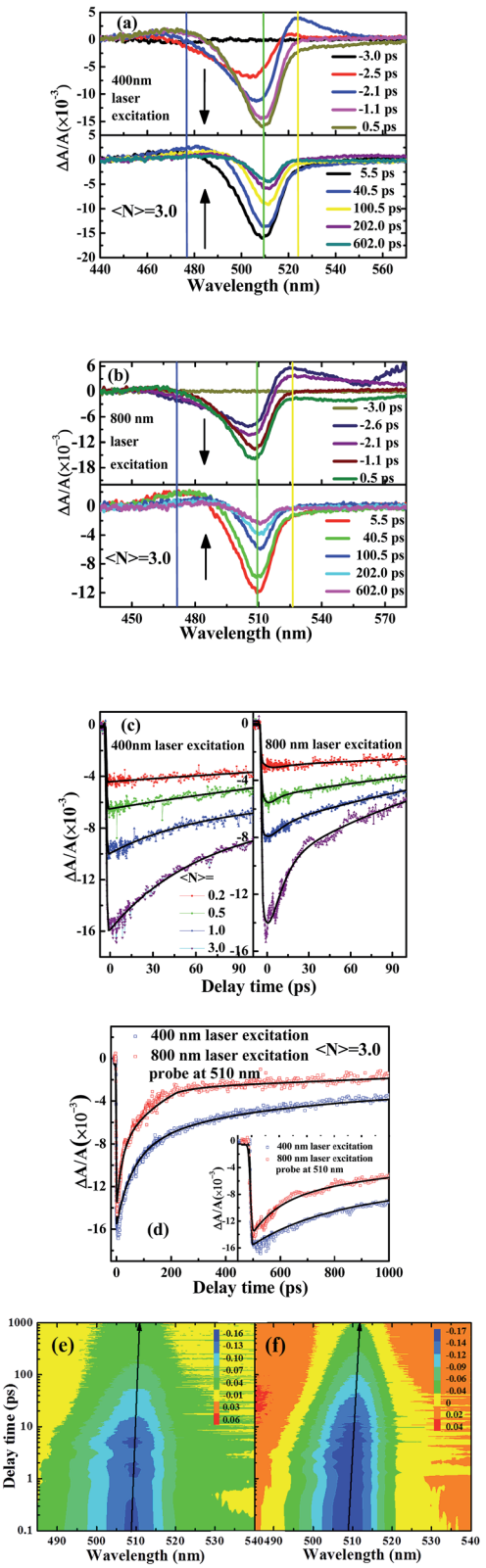

Fig. 5 (a) and (b) TA spectra of $CsPbBr_3$ NCs at various time delays under 400 nm and 800 nm laser excitation, respectively. (c) Dynamics traces under 400 nm and 800 nm laser excitation at various mean excitation numbers $\langle N \rangle$ in NCs. (d) Dynamics traces recorded at 510 nm under 400 nm and 800 nm laser excitation, respectively. Inset: dynamics traces of $CsPbBr_3$ NCs in the delay time window of −20 to 100 ps. (e) and (f) TA spectra contour of $CsPbBr_3$ NCs with the spectral range of 480–540 nm under 400 and 800 nm laser excitation at $\langle N \rangle = 3.0$.

recombination process is inevitably influenced by trapping states due to the trap-filling effect.[40] The early time TA spectra exhibit the typical signature of redshift for band-edge transition and observed spectral feature with photoinduced absorption at lower energies, and bleaching at higher. At longer times, as charges accumulate in the lowest energy states, the photoinduced absorption signal decays are replaced quickly by strong band-edge bleaching due to state filling.[41]

Through controlling the pump power intensity, the same $\Delta A/A$ intensity of $CsPbBr_3$ NCs can be collected under 400 nm and 800 nm laser excitation, respectively. Under 400 nm and 800 nm femtosecond laser excitation, the broad bleaching signal at 510 nm shows a redshift with delay time, suggesting that there are multiple relaxation pathways from the band-edge excited state after pump-laser excitation.[42] The TA spectra captured at various delay times show ~5 nm change in peak position, suggesting the involvement of more than a single excited state.[43] The "hot" exciton is injected into a NC, and the energy required to introduce the second exciton into the NC is reduced compared to the single-exciton state by exciton–exciton interaction.[41] This is a biexciton effect manifested by a redshift of band-edge transition. With increasing $\langle N \rangle$, the data show the faster component emerging due to the hot exciton relaxation,[39] as shown in Fig. 5(c) and (d). An increase in fluence leads to the appearance of fast component assigned to hot exciton relaxation (~tens of picosecond). It is found that the rate of hot exciton relaxation under 800 nm femtosecond laser excitation is faster than that of the 400 nm. Comparative investigation on ultrafast charge dynamics of organic–inorganic hybrid perovskite material under 400 nm and 800 nm laser excitation are discussed;[37] the presence of trapping states in the recombination process is confirmed due to the fluence-dependent charge decays. TA spectra contour of $CsPbBr_3$ NCs with the spectral range of 480–540 nm under 400 and 800 nm laser excitation at $\langle N \rangle = 3.0$ are shown in Fig. 5(e) and (f).

Another exciton state with lower energy is proposed to explain the redshift of band-edge transition with increasing delay time.[41,44] The time- and spectral-resolved TA data indicate that the trapping states in these $CsPbBr_3$ NCs are shallow near the excitonic states. These results provide deeper insights into the UCL and trapping states in $CsPbBr_3$ NCs. It indeed requires further study to clarify the influence of trapping states near the band-edge energy level for all-inorganic perovskite NCs.

4. Conclusions

In conclusion, upconversion luminescence in all-inorganic halide perovskite $CsPbBr_3$ NCs is studied by the use of time-resolved PL and TA spectroscopy. The redshift of peak position of upconversion luminescence is 3 nm with longer delay time. Time-resolved PL and TA spectroscopy under near-infrared femtosecond laser excitation demonstrate that FWHM and peak position are changed at various delay times, suggesting the existence of more than a single excited state. It can be found that UCL is composed of a photoinduced surface-trapping and a band-edge excitonic state and causes the observed biexponential dynamics. We conclude that the

redshift of the emission peak is caused by the relative change in luminescent intensity between excitonic and trapping states. These results provide more understanding of the underlying photophysics in $CsPbBr_3$ NC materials and are necessary for the optimization of LEDs in the future.

Acknowledgements

This work is supported by the National Natural Science Foundation of China (grant numbers 11304058, 61204007, and 11404307) and NSAF (grant number U1330106). This work is partially supported by Fundamental Research Funds for the central Universities and Program for Innovation Research of Science in Harbin Institute of Technology (PIRS OF HIT 201621); New-Century Training Programme Foundation for the Talents by Heilongjiang Province (1254-NCET-018); Foundation for University Key Teacher by Heilongjiang Province (1252G047); Heilongjiang Province Postdoctoral Science Foundation (LBH-Q14139); Science Foundation of Heilongjiang University for Young Scholars (JCL201205).

References

1 W. S. Yang, J. H. Noh, N. J. Jeon, Y. C. Kim, S. Ryu, J. Seo and S. I. Seok, *Science*, 2015, **348**, 1234–1237.
2 P. Ramasamy, D.-H. Lim, B. Kim, S.-H. Lee, M.-S. Lee and J.-S. Lee, *Chem. Commun.*, 2016, **52**, 2067–2070.
3 S. Yakunin, L. Protesescu, F. Krieg, M. I. Bodnarchuk, G. Nedelcu, M. Humer, G. De Luca, M. Fiebig, W. Heiss and M. V. Kovalenko, *Nat. Commun.*, 2015, **6**, 8056.
4 Z.-K. Tan, R. S. Moghaddam, M. L. Lai, P. Docampo, R. Higler, F. Deschler, M. Price, A. Sadhanala, L. M. Pazos, D. Credgington, F. Hanusch, T. Bein, H. J. Snaith and R. H. Friend, *Nat. Nanotechnol.*, 2014, **9**, 687–692.
5 Y. Xu, Q. Chen, C. Zhang, R. Wang, H. Wu, X. Zhang, G. Xing, W. W. Yu, X. Wang, Y. Zhang and M. Xiao, *J. Am. Chem. Soc.*, 2016, **138**, 3761–3768.
6 L. Protesescu, S. Yakunin, M. I. Bodnarchuk, F. Krieg, R. Caputo, C. H. Hendon, R. X. Yang, A. Walsh and M. V. Kovalenko, *Nano Lett.*, 2015, **15**, 3692–3696.
7 F. Zhang, H. Zhong, C. Chen, X.-G. Wu, X. Hu, H. Huang, J. Han, B. Zou and Y. Dong, *ACS Nano*, 2015, **9**, 4533–4542.
8 D. N. Dirin, L. Protesescu, D. Trummer, I. V. Kochetygov, S. Yakunin, F. Krumeich, N. P. Stadie and M. V. Kovalenko, *Nano Lett.*, 2016, **16**, 5866–5874.
9 M. Haase and H. Schaefer, *Angew. Chem., Int. Ed.*, 2011, **50**, 5808–5829.
10 W. Wu, Y. Gao, Q. Chang, H. Ye, Z. Zheng, W. Liu, A. Li and Y. Yang, *J. Nanopart. Res.*, 2011, **13**, 1049–1061.
11 A. Javier, D. Magana, T. L. Jennings and G. F. Strouse, *Appl. Phys. Lett.*, 2003, **83**, 1423–1425.
12 X. Li, Y. Wu, S. Zhang, B. Cai, Y. Gu, J. Song and H. Zeng, *Adv. Funct. Mater.*, 2016, **26**, 2435–2445.
13 J. Pan, S. P. Sarmah, B. Murali, I. Dursun, W. Peng, M. R. Parida, J. Liu, L. Sinatra, N. Alyami, C. Zhao, E. Alarousu, T. K. Ng, B. S. Ooi, O. M. Bakr and O. F. Mohammed, *J. Phys. Chem. Lett.*, 2015, **6**, 5027–5033.
14 L. Protesescu, S. Yakunin, M. I. Bodnarchuk, F. Bertolotti, N. Masciocchi, A. Guagliardi and M. V. Kovalenko, *J. Am. Chem. Soc.*, 2016, **138**, 14202–14205.
15 L. C. Schmidt, A. Pertegas, S. Gonzalez-Carrero, O. Malinkiewicz, S. Agouram, G. Minguez Espallargas, H. J. Bolink, R. E. Galian and J. Perez-Prieto, *J. Am. Chem. Soc.*, 2014, **136**, 850–853.
16 K. Zheng, K. Zidek, M. Abdellah, M. E. Messing, M. J. Al-Marri and T. Pullerits, *J. Phys. Chem. C*, 2016, **120**, 3077–3084.
17 B. A. Koscher, J. K. Swabeck, N. D. Bronstein and A. P. Alivisatos, *J. Am. Chem. Soc.*, 2017, **139**, 6566–6569.
18 Y. Wang, Y. Wang, S. Dev Verma, M. Tan, Q. Liu, Q. Yuan, N. Sui, K. Zhihui, Z. Qiang and Z. Han-Zhuang, *Appl. Phys. Lett.*, 2017, **110**, 5.
19 Y. Wang, X. Li, X. Zhao, L. Xiao, H. Zeng and H. Sun, *Nano Lett.*, 2016, **16**, 448–453.
20 C. C. Stoumpos, C. D. Malliakas, J. A. Peters, Z. Liu, M. Sebastian, J. Im, T. C. Chasapis, A. C. Wibowo, D. Y. Chung, A. J. Freeman, B. W. Wessels and M. G. Kanatzidis, *Cryst. Growth Des.*, 2013, **13**, 2722–2727.
21 P. Cottingham and R. L. Brutchey, *Chem. Mater.*, 2016, **28**, 7574–7577.
22 Y. Wang, T. Van Duong, Y. Gao, T. C. He, R. Chen, E. Mutlugun, H. V. Demir and H. D. Sun, *Adv. Mater.*, 2014, **26**, 2954–2961.
23 W. Zhang, D. Dai, X. Chen, X. Guo and J. Fan, *Appl. Phys. Lett.*, 2014, **104**, 91902.
24 V. D'Innocenzo, G. Grancini, M. J. P. Alcocer, A. R. S. Kandada, S. D. Stranks, M. M. Lee, G. Lanzani, H. J. Snaith and A. Petrozza, *Nat. Commun.*, 2014, **5**, 3586.
25 J. Xing, X. F. Liu, Q. Zhang, S. T. Ha, Y. W. Yuan, C. Shen, T. C. Sum and Q. Xiong, *Nano Lett.*, 2015, **15**, 4571–4577.
26 T. J. Savenije, C. S. Ponseca Jr, L. Kunneman, M. Abdellah, K. Zheng, Y. Tian, Q. Zhu, S. E. Canton, I. G. Scheblykin, T. Pullerits, A. Yartsev and V. Sundstrom, *J. Phys. Chem. Lett.*, 2014, **5**, 2189–2194.
27 K. Wu, A. Bera, C. Ma, Y. Du, Y. Yang, L. Li and T. Wu, *Phys. Chem. Chem. Phys.*, 2014, **16**, 22476–22481.
28 J. Li, X. Yuan, P. Jing, J. Li, M. Wei, J. Hua, J. Zhao and L. Tian, *RSC Adv.*, 2016, **6**, 78311–78316.
29 A. Al Salman, A. Tortschanoff, M. B. Mohamed, D. Tonti, F. van Mourik and M. Chergui, *Appl. Phys. Lett.*, 2007, **90**, 093104.
30 D. Priante, I. Dursun, M. S. Alias, D. Shi, V. A. Melnikov, T. K. Ng, O. F. Mohammed, O. M. Bakr and B. S. Ooi, *Appl. Phys. Lett.*, 2015, **106**, 81902.
31 S. Seth, N. Mondal, S. Patra and A. Samanta, *J. Phys. Chem. Lett.*, 2016, **7**, 266–271.
32 A. R. S. Kandada, S. Neutzner, V. D'Innocenzo, F. Tassone, M. Gandini, Q. A. Akkerman, M. Prato, L. Manna, A. Petrozza and G. Lanzani, *J. Am. Chem. Soc.*, 2016, **138**, 13604–13611.
33 S. Gonzalez-Carrero, L. Frances-Soriano, M. Gonzalez-Bejar, S. Agouram, R. E. Galian and J. Perez-Prieto, *Small*, 2016, **12**, 5245–5250.
34 N. Mondal and A. Samanta, *Nanoscale*, 2017, **9**, 1878–1885.

35 L. Yan, J. Yue, J. Si and X. Hou, *Opt. Express*, 2008, **16**, 12069–12074.
36 K. Zheng, K. Zidek, M. Abdellah, J. Chen, P. Chabera, W. Zhang, M. J. Al-Marri and T. Pullerits, *ACS Energy Lett.*, 2016, **1**, 1154–1161.
37 P. Piatkowski, B. Cohen, S. Kazim, S. Ahmad and A. Douhal, *Phys. Chem. Chem. Phys.*, 2016, **18**, 27090–27101.
38 J. S. Manser, J. A. Christians and P. V. Kamat, *Chem. Rev.*, 2016, **116**, 12956–13008.
39 Q. Liu, Y. Wang, N. Sui, Y. Wang, X. Chi, Q. Wang, Y. Chen, W. Ji, L. Zou and H. Zhang, *Sci. Rep.*, 2016, **6**, 29442.
40 S. D. Stranks, V. M. Burlakov, T. Leijtens, J. M. Ball, A. Goriely and H. J. Snaith, *Phys. Rev. Appl.*, 2014, **2**, 034007.
41 N. S. Makarov, S. Guo, O. Isaienko, W. Liu, I. Robel and V. I. Klimov, *Nano Lett.*, 2016, **16**, 2349–2362.
42 M. J. Simpson, B. Doughty, B. Yang, K. Xiao and Y.-Z. Ma, *J. Phys. Chem. Lett.*, 2015, **6**, 3041–3047.
43 A. Swarnkar, R. Chulliyil, V. K. Ravi, M. Irfanullah, A. Chowdhury and A. Nag, *Angew. Chem., Int. Ed.*, 2015, **54**, 15424–15428.
44 J. Chen, D. Liu, M. J. Al-Marri, L. Nuuttila, H. Lehtivuori and K. Zheng, *Sci. China Mater.*, 2016, **59**, 719–727.

